1 **Overpressure generating mechanisms in the Peciko Field, Lower Kutai Basin, Indonesia**

2 Agus M. Ramdhan[1*] and Neil R. Goulty[1]

3 [1]*Department of Earth Sciences, Durham University, South Road, Durham DH1 3LE, UK*

4 *Corresponding author (e-mail: a.m.ramdhan@dur.ac.uk)*

5

6 **Running title:** Overpressure generating mechanisms in the Peciko Field

7

8 **ABSTRACT:** The Peciko Field contains gas in multiple stacked reservoirs within a Miocene

9 deltaic sequence. In the deeper reservoirs, gas is trapped hydrodynamically by high lateral

10 overpressure gradients. We have analysed overpressure and compaction in this field by using

11 wireline log, pressure, temperature, and vitrinite reflectance data. The top of overpressure is

12 located below 3 km burial depth, below the depth range for transformation of discrete

13 smectite to mixed-layer illite/smectite. Density-sonic and density-resistivity crossplots for

14 mudrocks show reversals within the transition zone into hard overpressure below 3.5 km

15 depth. Vitrinite reflectance measurements indicate that the start of unloading coincides with

16 the onset of gas generation. Moreover, mudrock density continues to increase with depth in

17 the overpressured section to values above 2.6 g cm^{-3}. We conclude that gas generation and

18 chemical compaction are responsible for overpressure generation, contradicting previous

19 interpretations that disequilibrium compaction is the principal mechanism for generating

20 overpressure in the Lower Kutai Basin. The particular circumstances which make our radical

21 interpretation plausible are that it is a warm basin with lateral reservoir drainage, so the

22 overpressured mudrocks are probably overcompacted as a result of diagenesis.

23

24 **KEYWORDS:** *Lower Kutai Basin, overpressure, unloading, gas generation, compaction*

25

Introduction

Overpressure in Cenozoic basins is commonly associated with the inability of fluid to escape rapidly enough to remain in hydrostatic equilibrium during ongoing burial. As a consequence, the sediments retain higher porosities than they would do if the pore pressure were hydrostatic. This process is referred to as disequilibrium compaction (Swarbrick *et al*. 2002). Disequilibrium compaction was recognized as a primary mechanism for generating overpressure in the US Gulf Coast region over 40 years ago (Pennebaker 1968; Reynolds 1970). Since then, disequilibrium compaction has been diagnosed as the cause of overpressure in many sedimentary basins worldwide, including the Neogene prodelta mudrocks of the Baram Delta, Brunei (Tingay *et al.* 2009).

More recent work in overpressure analysis has shown the importance of other overpressure generating mechanisms apart from disequilibrium compaction, even in Neogene sequences. These overpressure generating mechanisms, such as gas generation, clay diagenesis, aquathermal pressuring and pressure transference, can be classified as unloading mechanisms (Bowers 1995). Some examples of basins where these mechanisms have been shown to be active are Haltenbanken and the Northern North Sea (Hermanrud *et al*. 1998; Teige *et al*. 1999, 2007), the Eugene Island area of the Gulf of Mexico (Bowers 2001), and the inner shelf sequence of the Baram Delta (Tingay *et al*. 2009).

The Peciko Field is located within Miocene strata in the Lower Kutai Basin, Kalimantan, Indonesia (Fig. 1). A transition zone into hard overpressure is encountered in the field at depths of 11,000–14,000 ft (3350–4250 m). The primary mechanism responsible for overpressure generation in this area has previously been interpreted to be disequilibrium compaction (Bois *et al*. 1994; Bates 1996; Burrus 1998).

51

52   The principal objective of the work reported here was to determine whether

53 disequilibrium compaction really is the mechanism responsible for generating overpressure in

54 the Peciko Field. A secondary aim was to find a method which can be used during drilling

55 mudrock sections to estimate overpressure for wider application in the basin. By analysing

56 wireline log data in the mud-rich intervals, we show that overpressure is generated by

57 unloading mechanisms, probably including both gas generation and clay mineral diagenesis,

58 and not disequilibrium compaction. Our interpretation is radically different from that of

59 previous workers, who have all concluded that the principal mechanism for generating

60 overpressure was disequilibrium compaction.

61

62   In the following sections, we give background on the geology of the basin,

63 overpressure distribution, and wireline log responses to overpressure before presenting our

64 analysis of log, pressure, temperature, and vitrinite reflectance data. We then discuss the

65 implications for overpressure generation mechanisms and, in reaching our conclusions,

66 comment on the particular circumstances in the Lower Kutai Basin which make it a rewarding

67 basin to study for understanding overpressure generation and chemical compaction in mud-

68 rich sedimentary successions.

69

70 **Geological background and overpressure distribution**

71 Tectonically, the Lower Kutai Basin has experienced several episodes of rift, sag, and

72 inversion resulting from interaction between the Eurasia plate to the north, the Pacific Plate to

73 the east, and the Australian Plate to the south (Moss & Chambers 1999). The main inversion

74 episodes have occurred from the Middle Miocene to the present, and have been responsible

75 for the development of anticlinal structures (Chambers *et al*. 2004). The major structural

76   feature is the Samarinda Anticlinorium, consisting of a series of anticlines and synclines with

77   axes oriented approximately north–south. This anticlinorium is highly folded and faulted on

78   the onshore area, whereas dips are gentle in the shallow water and deep offshore areas. The

79   main north–south anticlinal folds are the Onshore Axis, Internal Axis, Median Axis, External

80   Axis, and Offshore Axis (Fig. 1). The Peciko Field is located on the Median Axis.

81

82   According to Allen & Chambers (1998), the thickness of the Neogene section in the

83   basin, which comprises deltaic sediment sourced by the Mahakam River in eastern

84   Kalimantan, may reach about 14 km in the depocentre. The Mahakam Delta is a fluvial-tidal

85   mud-dominated delta that has been prograding from the Early Miocene to the present day.

86   Stratigraphically, the productive interval in the Middle–Upper Miocene succession is the

87   Tunu Main Zone, and the hydrocarbons present are mainly gas. The Tunu Main Zone is sub-

88   divided into six intermediate stratigraphic units, of which only the uppermost five are present

89   in the Peciko Field. They have an average thickness of 300–400 m, based on the presence of

90   third-order maximum flooding surfaces. The intermediate stratigraphic units are further sub-

91   divided into several smaller stratigraphic units, based on the presence of local flooding

92   surfaces. The reservoirs in this field are dominantly distributary mouth bars (Samson *et al*.,

93   2005). The dimensions of individual mouth bars are 1–3 m thick and 1500–4000 m wide, and

94   stacked mouth bars attain thicknesses of 10–30 m (Fig. 2a). Figure 2b is a schematic cross-

95   section of the field which illustrates the stacked nature of the gas reservoirs and the tilted gas-

96   water contacts in the deeper overpressured accumulations.

97

98   The burial history of the Tunu Main Zone in this field (Fig. 3) shows that the

99   sedimentation rate during the last 8 My has been fairly constant at around 300 m My^{-1}. This

100 ongoing deposition of fine-grained sediment has previously been interpreted as being

101   responsible for the generation of overpressure by disequilibrium compaction in this area (Bois

102   *et al.* 1994; Bates 1996; Burrus 1998).

103

104   The inversion episodes have caused almost all of the Neogene sedimentary layers to

105   crop out in the onshore and coastal areas. Consequently, overpressure can bleed off laterally

106   on the basin scale, depending on the degree of reservoir connectivity. This process is known

107   as lateral reservoir drainage (O'Connor & Swarbrick 2008). The occurrence of lateral

108   reservoir drainage in the Peciko Field was identified by Grosjean *et al.* (1994) and Lambert *et*

109   *al.* (2003). The lateral overpressure gradients are sufficiently large to create hydrodynamic

110   traps for gas. For example, in stratigraphic unit 3 the lateral overpressure gradient reaches 150

111   psi km^{-1} (Fig. 4a). Given a gas density of 0.2 g cm^{-3}, the gas-water contact has a tilt of up to

112   7°. There is ample field evidence of tilted accumulations of gas in the deeper reservoir

113   intervals of the Peciko Field. In these reservoirs, the gas accumulations are displaced down-

114   dip on to the northern flank of the structure, as shown schematically in Fig. 2b, and the gas

115   column in crestal wells is either very thin or absent (Fig. 4b). A south–north cross-section

116   (Fig. 5) shows that both top of overpressure and the top of the pressure transition zone deepen

117   to the north, where the strata are more sand-rich.

118

119   Information about source rocks in the Lower Kutai Basin generally, and in the Peciko

120   Field specifically, has been provided by Oudin & Picard (1982), Schoell *et al.* (1985), Burrus

121   *et al.* (1992), Paterson *et al.* (1997), Duval *et al.* (1998), and Lambert *et al.* (2003). The main

122   source rocks in the area are organic-rich mudrocks, coal beds, and even sandy facies

123   deposited in fluvial, deltaic top, tidal plain, and delta front settings. They are mostly classified

124   as Type III source rocks. Although the organic-rich mudrocks are gas prone, Lambert *et al.*

125   (2003) reported that the oil-generative potential of the Type III organic matter is unusually

126   high. The contribution to hydrocarbon generation from marine mudrocks, located in the

127   deepwater Makassar Straits and in the deeper part of fields surrounding Mahakam Delta, is

128   thought to be negligible because their organic content is low. Interestingly, isotopic analysis

129   performed by Lambert *et al*. (2003) showed that the threshold for both gas and oil maturation

130   corresponds to a vitrinite reflectance of 0.6%.

131

132   **Wireline log responses to overpressure**

133   There are several candidate mechanisms for generating overpressure in the Lower Kutai

134   Basin, including disequilibrium compaction, clay diagenesis, gas generation, and lateral

135   pressure transfer. Wireline log analysis can help to distinguish between these mechanisms

136   (e.g. Bowers 2001; Katahara 2006).

137

138   When a mud-rich sedimentary succession cannot dewater rapidly enough for the pore

139   pressure to remain hydrostatic during burial, its porosity is greater than that it would be if the

140   pore pressure were hydrostatic, and the overpressure is said to be caused by disequilibrium

141   compaction. Where overpressure has been generated by disequilibrium compaction in a

142   uniform mudrock succession, with virtually no loss of pore fluid, the porosity remains

143   constant and the pore pressure-depth profile becomes parallel to the vertical stress-depth

144   profile.

145

146   Where overpressure has been generated by an unloading mechanism such as clay

147   diagenesis, gas generation or lateral transfer, the pore pressure can increase more rapidly with

148   depth than the vertical stress (Fig. 6). In such circumstances, the density usually continues to

149   increase with depth through the overpressured mudrocks, while the sonic log trend reverses,

150   moving towards higher sonic travel time with increasing depth. The resistivity log trend also

151   reverses, moving towards lower resistivity with increasing depth. These responses can be

152   explained by the concept of storage pores and connecting pores (Bowers & Katsube 2002).

153   When pore pressure in a mudrock increases due to fluid expansion, the unloading response is

154   essentially elastic and results in only a very small increase in porosity. Because the density

155   log measures the bulk porosity of the mudrock, it is barely affected by the fluid expansion.

156   The increase in porosity that does occur during fluid expansion is predominately due to the

157   opening of flat connecting pores, because they are more compliant than the storage pores. The

158   sonic and resistivity log responses are sensitive to the opening of connecting pores because

159   their opening reduces the bulk modulus and rigidity and increases the conductivity.

160

161   **Data analysis**

162   The Peciko Field was developed using the concept of hydrodynamic trapping (Grosjean *et al*.

163   1994; Lambert *et al*. 2003), and a campaign of reservoir pressure measurements for

164   hydrodynamic analysis purposes has resulted in an excellent pressure database. On average,

165   there are around 70 RFT points in each well. These pressure data are very useful for

166   overpressure analysis because they can be used both to determine overpressure distribution

167   and to calibrate methods of pore pressure estimation.

168

169   We have analysed data from the discovery well, PEC-1, and 16 appraisal wells in the

170   Peciko Field, most of which have terminated at the pressure transition zone into hard

171   overpressure. Here, we present data from three wells, PEC-1, NWP-9, and NWP-16 (Fig. 2a),

172   to illustrate our findings. PEC-1 was chosen as a typical example of a well on the crest of the

173   structure and because source rock maturation data are available from it, although it does

174   contain a relatively small number of RFT points and no density log was run in this early well.

175   NWP-9 was chosen because it encounters the highest overpressure value in the Peciko Field

176   and shows a clear unloading response on density-sonic and density-resistivity crossplots.

177   NWP-16 is located downflank in the northern part of the field where the top of overpressure is

178   deeper and the geothermal gradient is slightly lower (Fig. 3). It is the deepest well in the field

179   and was chosen to make a comparison of the wireline log responses with those from well

180   NWP-9.

181

182   Prior to analysing the wireline response to overpressure, it is necessary to discriminate

183   mud-rich intervals from more silty and sandy intervals from the given set of wireline logs.

184   Discrimination was done by cross-plotting density against the difference between neutron

185   porosity and the porosity estimated from the density logs (Fig. 7), as done by Katahara

186   (2006). To infer porosity from the density log, a matrix density of 2.75 g cm^{-3} and a fluid

187   density of 1.05 g cm^{-3} were arbitrarily assumed. An arbitrary threshold value of 0.18 was

188   chosen (i.e., NPHI – DPHI > 0.18) to ensure that our pressure analysis was consistently

189   performed in the mud-rich intervals, although tests showed that estimated pore pressures in

190   the mudrocks had low sensitivity to the choice of threshold value.

191

192   The pressure-depth plot for well PEC-1 (Fig. 8a) is typical of wells in this field, except

193   that the top of overpressure is located at slightly greater depths further north (Fig. 3). The

194   overpressure initially increases slowly with depth below the top of overpressure at ~9500 ft

195   (~2900 m) and then more rapidly through a transition zone into hard overpressure. The top of

196   the transition zone is at ~11,300 ft (~3450 m). The top of transition zone is picked at the depth

197   where vertical effective stress starts to decrease as depth increases.

198

199   According to Lambert *et al.* (2003), the maturity threshold for gas generation

200   corresponds to a vitrinite reflectance value of 0.6%. Well PEC-1 is the only well in the

201   Peciko Field from which vitrinite reflectance data are available (Fig. 8b). There is a

202   correlation between the top of the transition zone into hard overpressure and the vitrinite

203   reflectance value of 0.6%. Four data points in the interval 10,000–12,000 ft (3050–3650 m)

204   have vitrinite reflectance values below the general trend. There is no other available

205   information to indicate whether they are reliable, but there is a possibility that these values

206   were obtained from fragments due to caving, and not cuttings from the drill bit.

207

208   The pressure-depth plot for well NWP-9 (Fig. 9) indicates that the top of overpressure

209   is at a depth of ~11,000 ft (~3350 m), although there is a good RFT measurement showing

210   ~300 psi (~2 MPa) of overpressure in an isolated sand body at ~10,000 ft (~3050 m) depth.

211   The top of the transition into hard overpressure is around 12,000 ft (3650 m) depth, where

212   reversals can be seen in the trends of both the sonic and resistivity logs through the mudrocks.

213   The density log, by contrast, shows no obvious reversal, but it shows consistently high values

214   of density, around 2.6 g cm^{-3}, in the depth interval 11,000–13,000 ft (3350–3950 m).

215

216   The pressure-depth plot for well NWP-16 (Fig. 10) appears to converge slightly

217   towards the lithostatic gradient with increasing depth, but it is not clear whether the well has

218   entered the expected transition zone into hard overpressure. The wireline logs appear to

219   display asymptotic trends towards the bottom of the well, without any clear indication of

220   reversals, although it is possible that the trends of both sonic and resistivity logs are on the

221   point of reversing at the bottom of the well.

222

223   Crossplots of density against sonic and resistivity log values for mudrocks in well

224   NWP-9 are shown in Fig. 11, with data points colour-coded at intervals of 1000 ft (305 m).

225   The smectitic and illitic compaction trends, introduced by Dutta (2002) and adopted by

226   Katahara (2006), are shown on the density-sonic crossplot for reference. The smectitic

227   compaction trend is followed by mudrocks with a high proportion of discrete smectite. The

228   illitic compaction trend is followed by mudrocks in which all the discrete smectite has been

229   transformed into mixed-layer illite/smectite. Both crossplots show clear unloading responses

230   starting at a depth of ~12,000 ft (~3650 m). The data points coloured red in the deepest

231   interval show changes in trend, with increased sonic transit time and decreased resistivity but

232   no decrease in density. These observations provide clear evidence that the generating

233   mechanism for hard overpressure is an unloading process. Data points in the depth range

234   5000–12,000 ft (1500–3650 m) on the density-sonic crossplot fall on, or close to, the illitic

235   compaction trend. The average geothermal gradient is around 0.0094 °C ft^{-1} (0.031°C m^{-1})

236   with a surface temperature of 30°C, giving an estimated temperature of nearly 80°C at 5000 ft

237   (1500 m) depth, sufficient for discrete smectite to have disappeared (Hower *et al*. 1976; Boles

238   & Franks 1979).

239

240   Clauer *et al*. (1999) investigated clay mineralogy in the Tunu Field, which is located

241   on the Median Axis north of Peciko (Fig. 1) so the clay mineralogy in the two fields may be

242   expected to be similar. At sampling depths below 7700 ft (2350 m), they found that the clay

243   fraction consists of mixed-layer illite/smectite, kaolinite/dickite, detrital illite and chlorite.

244   This clay mineral composition is consistent with the illitic compaction trend observed below

245   ~5000 ft (~1500 m) (Fig. 11). The fact that the density-sonic crossplot follows an illitic

246   compaction trend over the hydrostatically pressured depth interval of 5000–11,000 ft (1500–

247   3350 m) indicates that excess water which may have been released by the transformation of

248   discrete smectite to mixed-layer illite/smectite has dissipated and does not contribute to

249   present-day overpressures. However, clay diagenetic reactions that continue to be active at

250   higher temperatures, including ongoing illitization of mixed-layer illite/smectite and the

251   conversion of kaolinite to illite (Bjørlykke 1998), and also quartz dissolution and precipitation

252   (Bjørkum 1995), probably do contribute to present-day overpressures.

253

254   Composite density plots for mudrocks in all 16 NWP wells (Fig. 4a) are shown in Fig.

255   12, without and with the data points from the overpressured intervals in each well. The

256   density continues to increase smoothly below the top of overpressure, even though the vertical

257   effective stress reaches its maximum value at the top of overpressure in each well. Thus,

258   compaction appears to continue with increasing depth, independent of the vertical effective

259   stress. This plot constitutes strong evidence for ongoing chemical compaction below the top

260   of overpressure, and for discounting disequilibrium compaction as a mechanism that

261   contributes to the generation of overpressure in this field. Given the high average density, in

262   excess of 2.6 g cm^{-3} below 12,000 ft in all wells (Fig. 12), our preferred interpretation is that

263   the mudrocks in the overpressured intervals have become overcompacted by diagenetic

264   processes, i.e. overcompacted in a mechanical sense due to the chemical compaction

265   processes.

266

267   **Implications for overpressure generation**

268   Pressure-depth plots show that the top of overpressure is at depths of 9500–12,000 ft (2900–

269   3650 m), corresponding to estimated temperatures of 120–140°C, and that there is a transition

270   zone into hard overpressure at depths of 11,500–14,000 ft (3500–4250 m), corresponding to

271   estimated temperatures of 140–160°C. These depths to the top of overpressure are relatively

272   large in comparison to other Neogene basins worldwide, as summarized by Swarbrick *et al*.

273   (2002). For example, in the Malay Basin where the sedimentation rate is around 800 ft My^{-1}

274   (240 m My^{-1}), about 20% less than the sedimentation rate over the last 8 My in the Lower

275   Kutai Basin, the top of overpressure is around 3200 ft (975 m) depth. Presumably, the top of

276   overpressure in the Lower Kutai Basin is so deep because of lateral reservoir drainage

277   (Grosjean *et al*. 1994; Lambert *et al*. 2003). Inversion started in Middle Miocene times and

278   has continued to the present day with uplift centred on the onshore area (Chambers *et al*.

279   2004). Unpublished net-to-gross (NTG) maps for the Median Axis region of the Lower Kutai

280   Basin show a progressive upward increase in NTG at the Peciko Field from stratigraphic unit

281   5 up to stratigraphic unit 3 (Figs 2b and 5), which is consistent with effective lateral drainage

282   above the overpressured zone.

283

284   Within the transition zone into hard overpressure in well NWP-9, both density-sonic

285   and density-resistivity crossplots show clear unloading responses (Figs 9 and 11). Clay

286   diagenesis may contribute to the present-day overpressure in the Peciko Field. In the

287   hydrostatically pressured succession, data on the density-sonic crossplots lie on the illite-rich

288   compaction trend below ~5000 ft (~1500 m), and remain on this trend in the zone of low

289   overpressure (Fig. 10). Although discrete smectite is likely to have disappeared by 5000 ft

290   (1500 m) burial depth, where the temperature approaches 80°C, illitization of mixed-layer

291   illite/smectite is ongoing at greater depths to much higher temperatures (Hower *et al*. 1976;

292   Boles & Franks 1979). Kaolinite transforms to illite at temperatures ~130–140°C in basin

293   settings (Bjørlykke 1998) and can contribute to overpressure both through the release of free

294   water by the reaction and by transferring load from the grains to the pore fluid as mineral

295   grains are dissolved (Bjørlykke & Hoeg 1997). This temperature range roughly corresponds

296   to that estimated at the depth of the transition zone into high overpressure. Furthermore, the

297   dissolution of kaolinite and precipitation of illite may reduce porosity and permeability at this

298   depth, and thereby help to maintain high overpressure in the deeper strata.

299

300   Gas generation seems likely to be another unloading process responsible for the hard

301   overpressure, generated both directly from kerogen and from oil cracking to gas. According to

302   Lambert *et al*. (2003), gas generation starts at a vitrinite reflectance of 0.6%. We have one set

303   of vitrinite reflectance data in the Peciko Field, i.e. in PEC-1 where there is a correlation

304   between high overpressure and vitrinite reflectance values above 0.6% (Fig. 7). Oudin &

305   Picard (1982) found that there is a good correlation between the top of hard overpressure and

306   the increase in vitrinite reflectance in the Handil Field (Fig. 13), and Bates (1996) found a

307   similar correlation in the Nilam Field (Fig. 14). However, they did not draw any conclusions

308   about overpressure generation mechanisms from the vitrinite reflectance data. We note that

309   the data in each of those two wells show a strong correlation between the depth of transition

310   into hard overpressure and the onset of gas generation, assuming that the threshold for gas

311   generation corresponds to a vitrinite reflectance of 0.6%.

312

313   To the south and east of the Peciko Field, the sands within the Tunu Main Zone peter

314   out as the depositional environment changes from the shelf break setting to deep marine.

315   Since the organic carbon content of the deep marine sediment is low and its potential for

316   hydrocarbon generation is negligible, there is unlikely to be significant lateral transfer of

317   overpressure generated by gas generation in the synclinal area to the southeast, but there may

318   be lateral transfer of overpressure generated by diagenetic reactions.

319

320   In all wells with density logs, NWP-1 to NWP-16, the logged density values continue

321   gradually to increase downwards through the zone of low overpressure (Fig. 12), which is

322   consistent with ongoing chemical compaction. The top of overpressure is located deep within

323   the chemical compaction zone, where the effective stress appears to have no influence on

324   compaction and the mudrocks are likely to be stiffened by chemical compaction so that they

325   are overconsolidated (Bjørlykke & Hoeg 1997; Bjørlykke 1998, 1999). Consequently, we

326   attribute the origin of the low overpressures, above the transition zone into hard overpressure,

327   to passive transmission of pore fluid from the highly overpressured zone below.

328

329   **Conclusions**

330   Hard overpressure in the Peciko Field is generated by unloading mechanisms. The top of

331   overpressure is much deeper than the depth range where transformation of discrete smectite to

332   mixed-layer smectite/illite occurs, so the disappearance of smectite does not contribute to the

333   observed overpressure. The causes of the hard overpressure in the Peciko Field are likely to

334   be gas generation, illitization of mixed-layer illite/smectite, conversion of kaolinite to illite,

335   and dissolution and precipitation of quartz. We suggest that expulsion of fluid resulting from

336   gas generation and diagenesis in the zone of high overpressure maintains the hydrodynamic

337   flow through the reservoir layers containing gas accumulations.

338

339   Compaction continues below the top of overpressure, independent of vertical effective

340   stress, in all 16 wells where density logs have been run. This observation is clear evidence of

341   ongoing chemical compaction. The origin of the low overpressure above the transition zone

342   into high overpressure is probably due to vertical transfer from below. The transition zone

343   into hard overpressure can be recognized from sonic and resistivity log reversals, whether by

344   direct inspection of the logs or by crossplotting their responses against the density log.

345

346   The high mudrock densities, greater than 2.6 g cm^{-3}, at the top of overpressure indicate

347   that the mudrocks are overcompacted. Therefore, our preferred interpretation is that

348   disequilibrium compaction does not contribute to the overpressure. This conclusion is

349   radically new because all other studies of overpressured Neogene basins have suggested that

350　disequilibrium compaction has contributed to the overpressure, either directly or indirectly by

351　pressure transference. The particular circumstances in the Lower Kutai Basin which make our

352　interpretation plausible are that it is a warm basin with lateral reservoir drainage.

353　Consequently, the top of overpressure is unusually deep for a mud-rich sequence that has

354　undergone rapid burial over the last 10 My.

355

361

362　**References**

363

364　Allen, G. P. & Chambers, J. L. C. 1998. *Sedimentation in the Modern and Miocene Mahakam*

365　*Delta*. Field Trip Guide Book, Indonesian Petroleum Association, Jakarta.

366

367　Bates, J. A. 1996. Overpressuring in the Kutai Basin: distribution, origins, and implications

368　for the petroleum system. *In: Indonesian Petroleum Association, Proceedings 25th Annual*

369　*Convention*, 93-115.

370

371　Bjørkum, P. A. 1995. How important is pressure in causing dissolution of quartz in

372　sandstones? *Journal of sedimentary Research*, **66**, 147-154.

373

374   Bjørlykke, K. 1998. Clay mineral diagenesis in sedimentary basins: a key to the prediction of

375   rock properties: examples from the North Sea Basin. *Clay Minerals*, **33**, 15–34.

376

377   Bjørlykke, K. 1999. Principal aspects of compaction and fluid flow in mudstones. *In:* Aplin,

378   A.C., Fleet, A.J. & Macquaker, J.H.S. (eds) *Muds and Mudstones: Physical and Fluid-Flow*

379   *Properties*. Geological Society, London, Special Publications, **158**, 73-78.

380

381   Bjørlykke, K. & Høeg, K. 1997. Effects of burial diagenesis on stresses, compaction and fluid

382   flow in sedimentary basins. *Marine and Petroleum Geology*, **14**, 267-276.

383

384   Bois, M., Grosjean, Y. & de Pazzis, L. 1994. Shale compaction and abnormal pressure

385   evaluation application to the offshore Mahakam. *In: Indonesian Petroleum Association,*

386   *Proceedings 23rd Annual Convention*, 245-259.

387

388   Boles, J. R. & Franks, S. G. 1979. Clay diagenesis in Wilcox sandstones of southwest Texas:

389   implications of smectite diagenesis on sandstone cementation. *Journal of Sedimentary*

390   *Petrology*, **49**, 55-70.

391

392   Bowers, G. L. 1995. Pore pressure estimation from velocity data: accounting for overpressure

393   other than undercompaction. *SPE Drilling & Completion*, **10**(2), 89-95.

394

395   Bowers, G. L. 2001. Determining an appropriate pore-pressure estimation strategy. *Offshore*

396   *Technology Conference*, paper OTC 13042.

397

398   Bowers, G. L. & Katsube, T. J. 2002. The role of shale pore structure on the sensitivity of

399   wire-line logs to overpressure. *In:* Huffman, A.R. & Bowers, G.L. (eds), *Pressure Regimes in*

400   *Sedimentary Basins and their Prediction.* AAPG, Tulsa, Memoir **76**, 43-60.

401

402   Burrus, J. 1998. Overpressure models for clastic rocks, their relation to hydrocarbon

403   expulsion: a critical reevaluation. *In:* Law, B.E., Ulmishek, G.F. & Slavin, V.I. (eds)

404   *Abnormal Pressures in Hydrocarbon Environments.* AAPG, Tulsa, Memoir **70**, 35-63.

405

406   Burrus, J., Brosse, E., Choppin de Janvry, G., Grosjean, Y. & Oudin, J. L. 1992. Basin

407   modelling in the Mahakam Delta based on integrated 2D model Temispack. *In: Indonesian*

408   *Petroleum Association, Proceedings 21st Annual Convention*, 23-43.

409

410   Chambers, J. L. C., Carter, I., Cloke, R., Craig, J., Moss, S. J. & Paterson, D. W. 2004. Thin-

411   skinned and thick-skinned inversion-related thrusting – a structural model for the Kutai Basin,

412   Kalimantan, Indonesia. *In:* McClay, K.R. (ed.) *Thrust Tectonics and Hydrocarbon Systems.*

413   AAPG, Tulsa, Memoir **82**, 614-634.

414

415   Clauer, N., Rinckenbach, T., Weber, F., Sommer, F., Chaudhuri, S. & O'Neil, J. R. 1999.

416   Diagenetic evolution of clay minerals in oil-bearing Neogene sandstones and associated

417   shales, Mahakam Delta Basin, Indonesia. *AAPG Bulletin*, **83**, 62-87.

418

419   Dutta, N. C. 2002. Deepwater geohazard prediction using prestack inversion of large offset P-

420   wave data and rock model. *The Leading Edge*, **21**, 193-198.

421

422   Duval, B. C., Cassaigneau, C., Choppin de Janvry, G., Loiret, B., Leo, M., Alibi & Grosjean,

423   Y. 1998. Impact of the petroleum system approach to exploration and appraisal efficiency in

424   the Mahakam Delta. *In: Indonesian Petroleum Association, Proceedings 26th Annual*

425   *Convention*, 277-290.

426

427   Grosjean, Y., Choppin de Janvry, G. & Duval, B. C. 1994. Discovery of a giant in a mature

428   deltaic province: Peciko, Indonesia. Presented at the 14th World Petroleum Congress, May–

429   June 1994, Stavanger, Norway.

430

431   Hermanrud, C., Wensaas, L., Teige, G. M. G., Vik, E., Nordgård Bolås, H. M. & Hansen, S.

432   1998. Shale porosities from well logs on Haltenbanken (Offshore Mid-Norway) show no

433   influence of overpressuring. *In:* Law, B.E., Ulmishek, G.F. & Slavin, V.I. (eds.) *Abnormal*

434   *Pressures in Hydrocarbon Environments*. AAPG, Tulsa, Memoir **70**, 65-87.

435

436   Hower, J., Eslinger, E. V., Hower, M. E. & Perry, E. A. 1976. Mechanism of burial and

437   metamorphism of argillaceous sediment : 1. Mineralogical and chemical evidence. *Geological*

438   *Society of America Bulletin*, **87**, 725-737.

439

440   Katahara, K. 2006. Overpressure and shale properties: stress unloading or smectite-illite

441   transformation? *76th SEG Annual Meeting*, Expanded Abstracts, 1520-1524.

442

443   Lambert, B., Duval, B. C., Grosjean, Y., Umar, I. M. & Zaugg, P. 2003. The Peciko case

444   history: impact of an evolving geological model on the dramatic increase of gas reserves in

445   the Mahakam Delta. *In:* Halbouty, M.T. (ed.) *Giant Oil and Gas Fields of the Decade 1990–*

446   *1999*. AAPG, Tulsa, Memoir **78**, 297-320.

447

448 Moss, S. J. & Chambers, J. L. C. 1999. Depositional modelling and facies architecture of rift

449 and inversion episodes in the Kutai Basin, Kalimantan, Indonesia. *In: Indonesian Petroleum*

450 *Association, Proceedings 27th Annual Convention*, 467-486.

451

452 O'Connor, S. A. & Swarbrick, R. E. 2008. Pressure regression, fluid drainage and a

453 hydrodynamically controlled fluid contact in the North Sea, Lower Cretaceous, Britannia

454 Sandstone Formation. *Petroleum Geoscience*, **14**, 115-126.

455

456 Oudin, J. L. & Picard, P. F. 1982. Genesis of hydrocarbons in Mahakam Delta and the

457 relationship between their distribution and the overpressured zone. *In: Indonesian Petroleum*

458 *Association, Proceedings 11th Annual Convention*, 181-202.

459

460 Paterson, D. W., Bachtiar, A., Bates, J. A., Moon, J. A. & Surdam, R. C. 1997. Petroleum

461 system of the Kutei Basin, Kalimantan, Indonesia. *In: Indonesian Petroleum Association,*

462 *Proceedings Petroleum Systems of SE Asia and Australasia Conference*, 709-726.

463

464 Pennebaker, E. S. 1968. Seismic data indicate depth and magnitude of abnormal pressure.

465 *World Oil*, **166**, 73-82.

466

467 Reynolds, E. B. 1970. Predicting overpressure zones with seismic data. *World Oil*, **171**, 78-

468 82.

469

470   Samson, P., Dewi-Rochette, T. & Lescoeur, M. 2005. Peciko geological modeling: optimizing

471   fluid distribution and model resolution of a giant gas field in a shale-dominated deltaic

472   environment. Asia Pacific Oil & Gas Conference, SPE paper 93253.

473

474   Schoell, M. B., Durand, B. & Oudin, J. L. 1985. Migration of oil and gas in the Mahakam

475   Delta: evidence and quantitative estimate from isotope and biomarker studies. *In: Indonesian*

476   *Petroleum Association, Proceedings 14th Annual Convention*, 49-56.

477

478   Swarbrick, R. E., Osborne, M. J. & Yardley, G. S. 2002. Comparison of overpressure

479   magnitude resulting from the main generating mechanisms. *In:* Huffman, A.R. & Bowers,

480   G.L. (eds) *Pressure Regimes in Sedimentary Basins and their Prediction*. AAPG, Tulsa,

481   Memoir **76**, 1-12.

482

483   Teige, G. M. G., Hermanrud, C., Wensaas, L. & Nordgård Bolås, H. M. 1999. The lack of

484   relationship between overpressure and porosity in North Sea and Haltenbanken shales.

485   *Marine and Petroleum Geology*, **16**, 321-335.

486

487   Teige, G. M. G., Hermanrud, C., Wensaas, L. & Nordgård Bolås, H. M. 2007. Geological

488   constraints of pore pressure detection in shales from seismic data. *Basin Research*, **19**, 33-50.

489

490   Tingay, M. R. P., Hillis, R. R., Swarbrick, R. E., Morley, C. K. & Damit, A. R. 2009. Origin

491   of overpressure and pore-pressure prediction in the Baram province, Brunei. *AAPG Bulletin*,

492   **83**, 51-74.

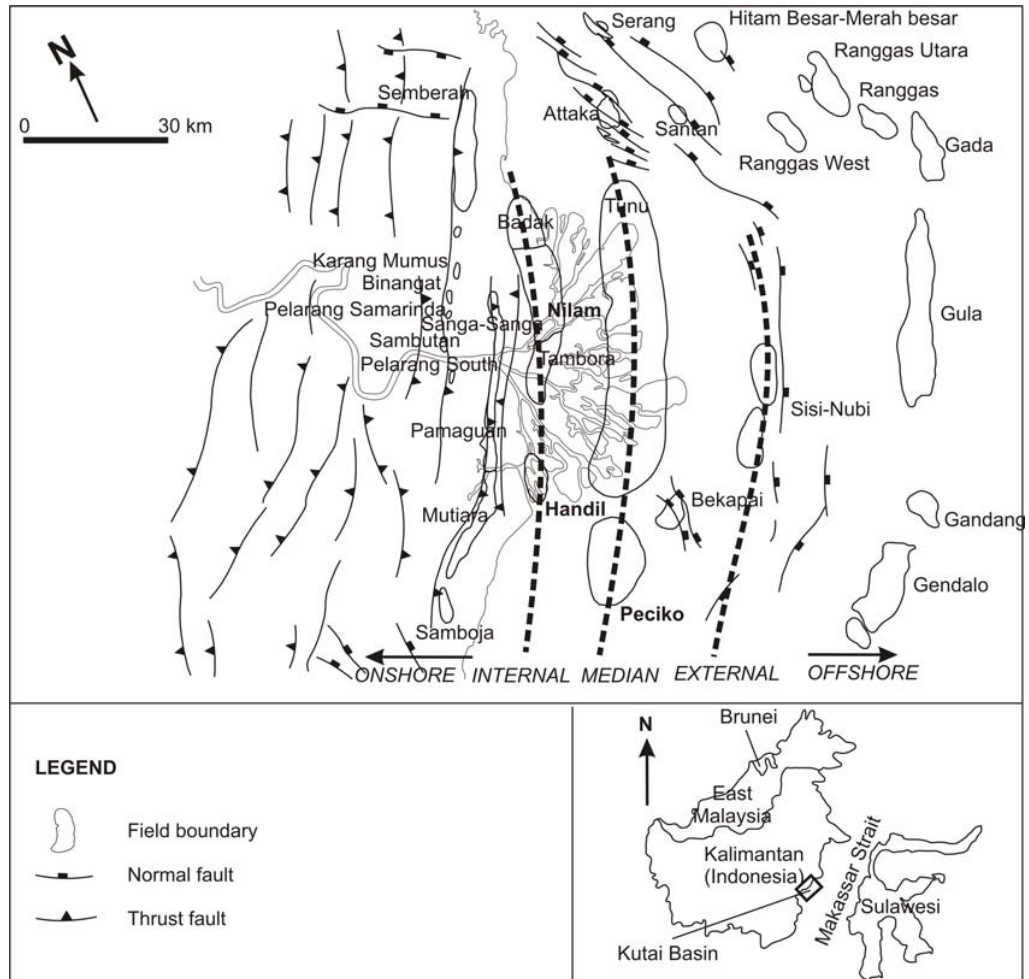493

494

Figure captions

496

497 Figure 1. Major structural features in the Lower Kutai Basin. The main north–south anticlines

498 are indicated by the outlines of known hydrocarbon accumulations.

499

500 Figure 2. Schematic sections through the Peciko Field at different vertical scales: (a) stacked

501 mouth bars in a stratigraphic interval between two local flooding surfaces (after Samson et al.,

502 2005); and (b) gas accumulations (red) with tilted GWCs in the Tunu Main Zone. SU1–SU5

503 are stratigraphic units of the Tunu Main Zone. A simplified lithological column for SU3 is

504 shown on the right: yellow denotes sand-rich intervals and green mudrock intervals.

505

506 Figure 3. Burial history of the Tunu Main Zone in the Peciko Field (modified from Lambert *et*

507 *al*. 2003).

508

509 Figure 4. (a) Lateral overpressure distribution in the uppermost reservoir of stratigraphic unit

510 3 in the Peciko Field before production started. Pressure data were taken from the discovery

511 well, PEC-1, and the 16 NWP appraisal wells. Overpressure contours are at intervals of 50

512 psi. The outline of the field indicates the lateral extent of gas accumulations in all units. (b)

513 Pore fluid distribution in the same stratigraphic unit showing that the gas accumulation is

514 located on the north flank of the structure. Red line: limit of the gas accumulation in this

515 stratigraphic unit. Red circles: wells where the reservoir is gas-bearing. Blue circles: wells

516 where this reservoir contains only water. Circle diameter is proportional to reservoir layer

517 thickness in each well. Structural contour interval is 82 ft (25 m).

518

519   Figure 5. South–north vertical section through the Peciko Field along the line marked in Fig.

520   4a showing the general trend of overpressure with depth.

521

522   Figure 6. Pressure-depth plot (right) with sonic and density log responses expected for a

523   mudrock succession where overpressure is generated by an unloading process. Below the top

524   of overpressure, the reversal in the trend of sonic transit time does not indicate abnormally

525   high porosity because density continues to increase with depth.

526

527   Figure 7. Crossplot of density against the difference between neutron and density porosities

528   estimated from wireline logs in well NWP-9. NPHI – DHPI = 0.18 was arbitrarily chosen as

529   the mudrock cut-off.

530

531   Figure 8. (a) Pressure-depth plot for well PEC-1. (b) Vitrinite reflectance data showing that

532   the threshold value of 0.6 % for gas generation, as determined by Lambert *et al*. (2003),

533   coincides with the top of the transition zone into hard overpressure. The encircled data points

534   are outliers from the trend and so may contain errors.

535

536   Figure 9. Pressure-depth plot for well NWP-9 with density, sonic, and resistivity log data for

537   the mudrocks.

538

539   Figure 10. Pressure-depth plot for well NWP-16 with density, sonic, and resistivity log data

540   for the mudrocks.

541

542   Figure 11. Crossplots of density against sonic transit time and resistivity for well NWP-9.

543   Data points on unloading trends are encircled in blue.

544

545   Figure 12. Composite density plot for mudrocks, defined by NPHI – DPHI > 0.18, in all the

546   NWP wells, Peciko Field: (a) for the hydrostatically pressured intervals only; and (b) for all

547   the density log data.

548

549   Figure 13. Vitrinite reflectance data and the pressure-depth plot from well H-9-B1 in the

550   Handil Field (location in Fig. 1). After Oudin & Picard (1982).

551

552   Figure 14. Vitrinite reflectance data from well N-109X in the Nilam Field (location in Fig. 1)

553   After Bates (1996).

Figure 1. Major structural features in the Kutai Basin. The main north–south anticlines are indicated by the outlines of known hydrocarbon accumulations.
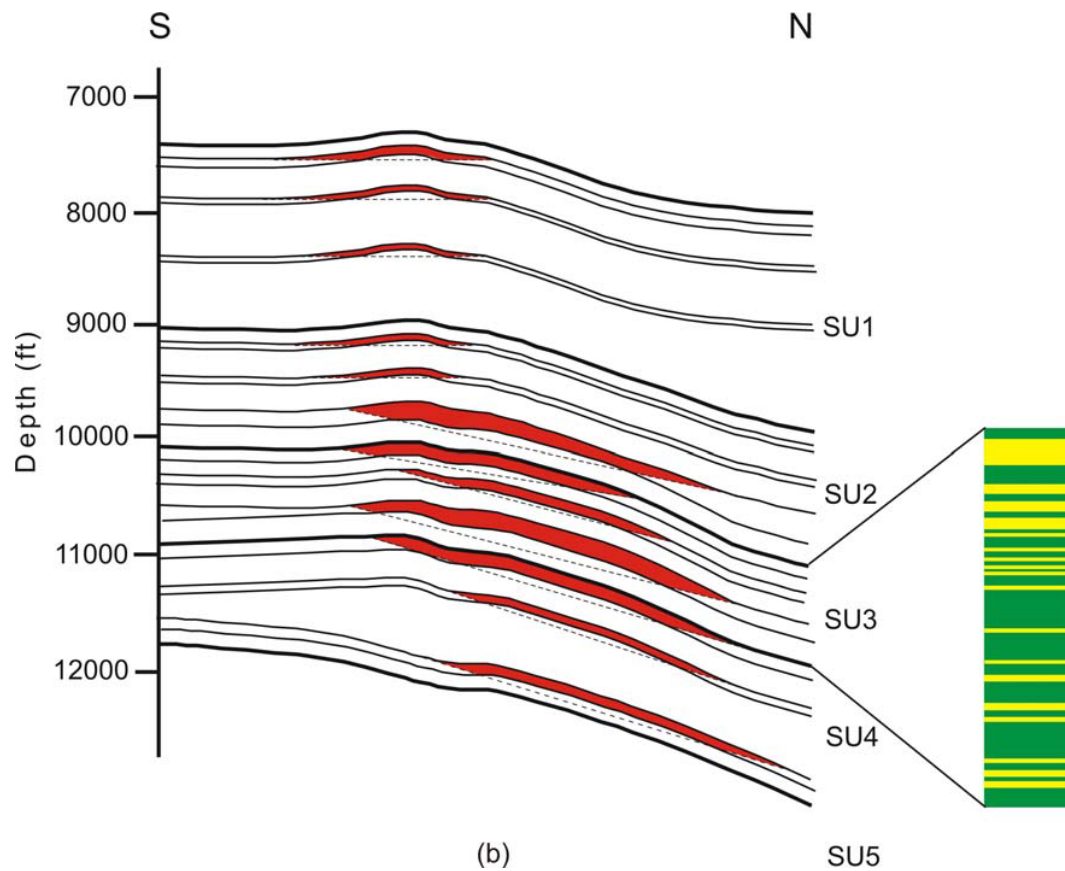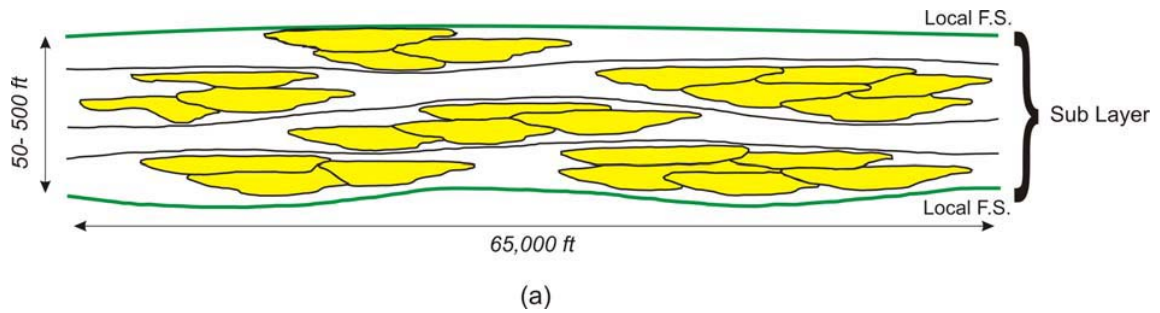
Figure 2. Schematic sections through the Peciko Field at different vertical scales: (a) stacked mouth bars in a stratigraphic interval between two local flooding surfaces (after Samson et al., 2005); and (b) gas accumulations (red) with tilted GWCs in the Tunu Main Zone. SU1–SU5 are stratigraphic units of the Tunu Main Zone. A simplified lithological column for SU3 is shown on the right: yellow denotes sand-rich intervals and green mudrock intervals.
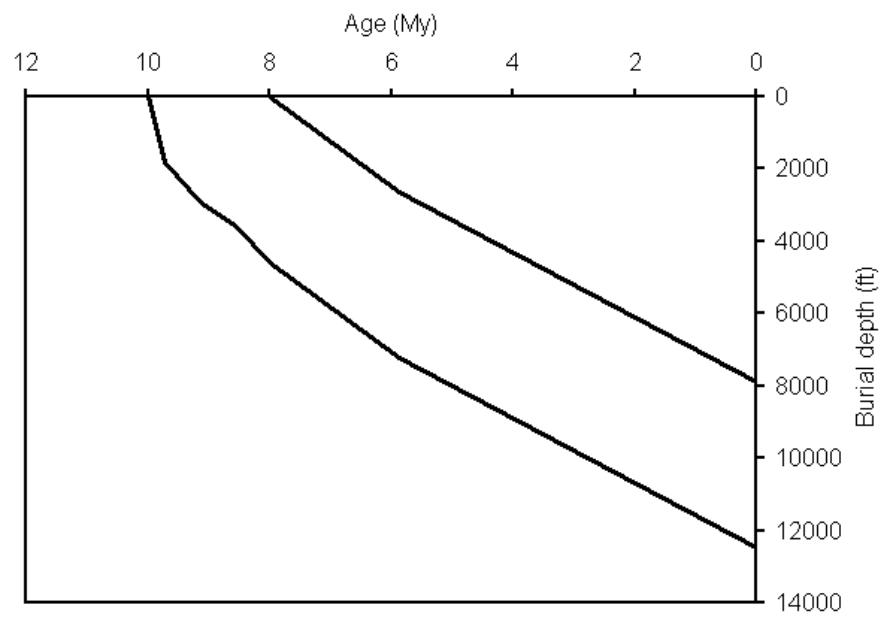
Figure 3. Burial history of Tunu Main Zone in the Peciko Field (modified from Lambert *et al*. 2003).
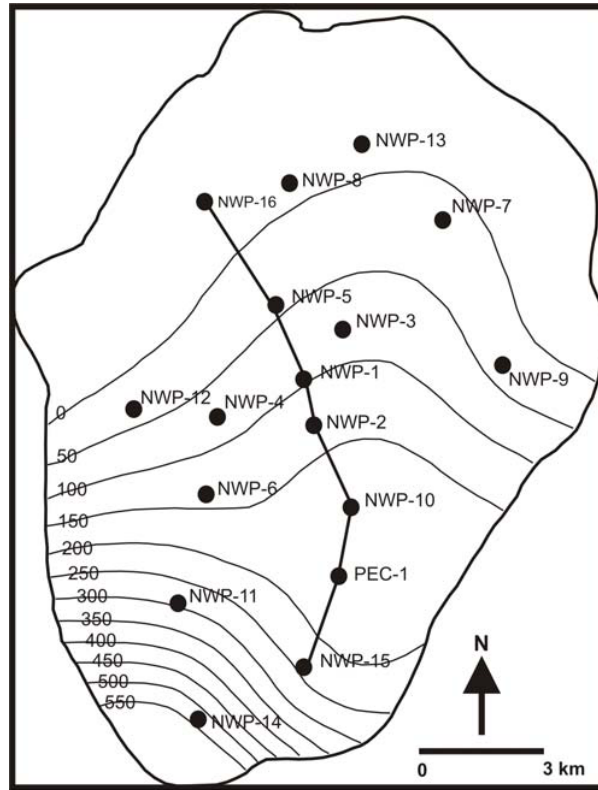
(a)
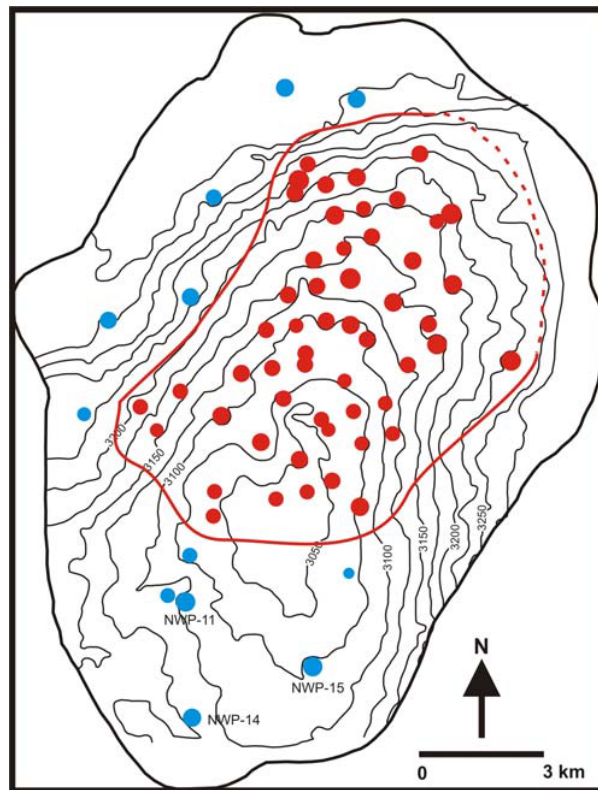
(b)

Figure 4. (a) Lateral overpressure distribution in the uppermost reservoir of stratigraphic unit 3 in the Peciko Field before production started. Pressure data were taken from the discovery well, PEC-1, and the 16 NWP appraisal wells. Overpressure contours are at intervals of 50 psi. The outline of the field indicates the lateral extent of gas accumulations in all units. (b) Pore fluid distribution in the same stratigraphic unit showing that the gas accumulation is located on the north flank of the structure. Red line: limit of the gas accumulation in this stratigraphic unit. Red circles: wells where the reservoir is gas-bearing. Blue circles: wells where this reservoir contains only water. Circle diameter is proportional to reservoir layer thickness in each well. Structural contour interval is 82 ft (25 m).
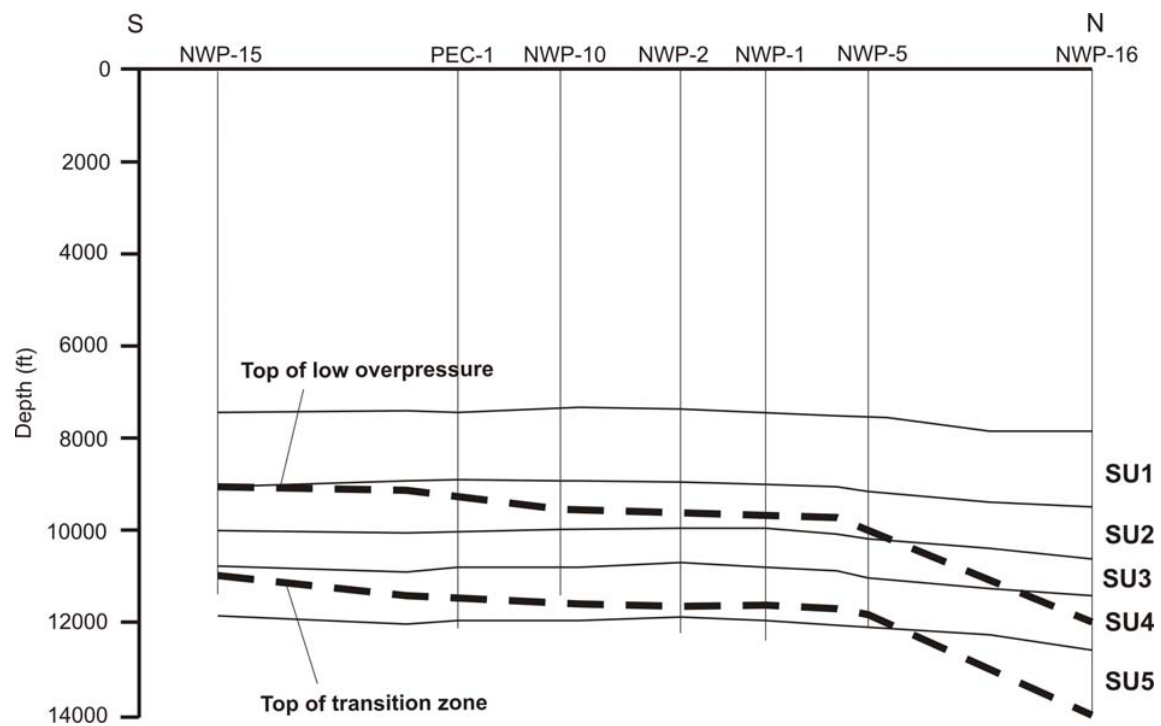
Figure 5. South–north vertical section through the Peciko Field along the line marked in Fig. 4a showing the general trend of overpressure with depth.
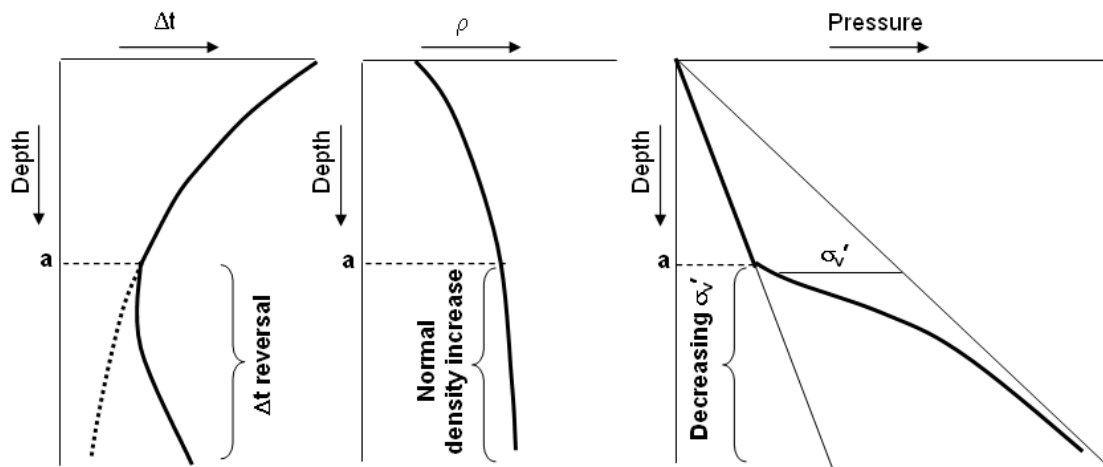
Figure 6. Pressure-depth plot (right) with sonic and density log responses expected for a mudrock succession where overpressure is generated by an unloading process. Below the top of overpressure, the reversal in the trend of sonic transit time does not indicate abnormally high porosity because density continues to increase with depth.
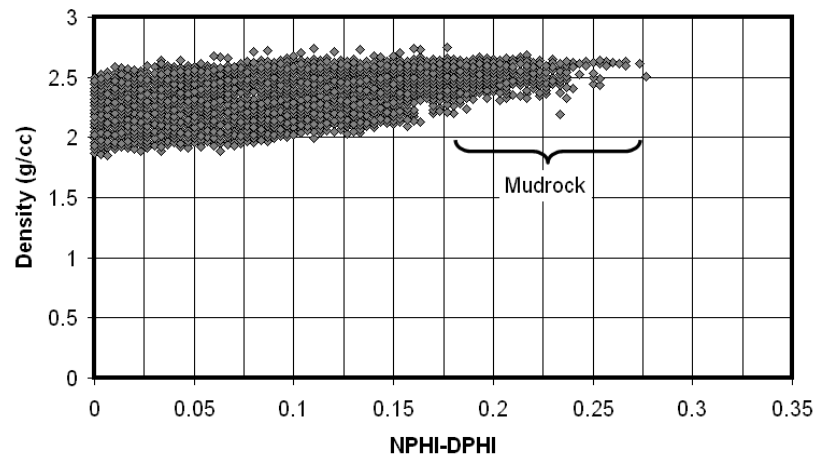
Figure 7. Crossplot of density against the difference between neutron and density porosities estimated from wireline logs in well NWP-9. NPHI – DHPI = 0.18 was arbitrarily chosen as the mudrock cut-off.
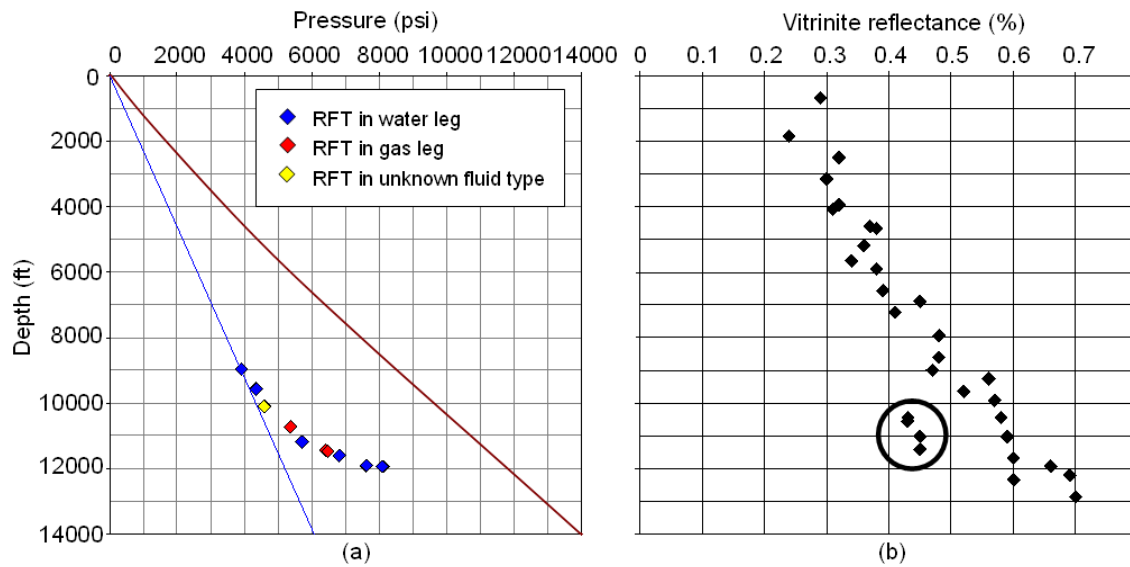
Figure 8. (a) Pressure-depth plot for well PEC-1. (b) Vitrinite reflectance data showing that the threshold value of 0.6 % for gas generation, as determined by Lambert *et al*. (2003), coincides with the top of the transition zone into hard overpressure. The encircled data points are outliers from the trend and so may contain errors.
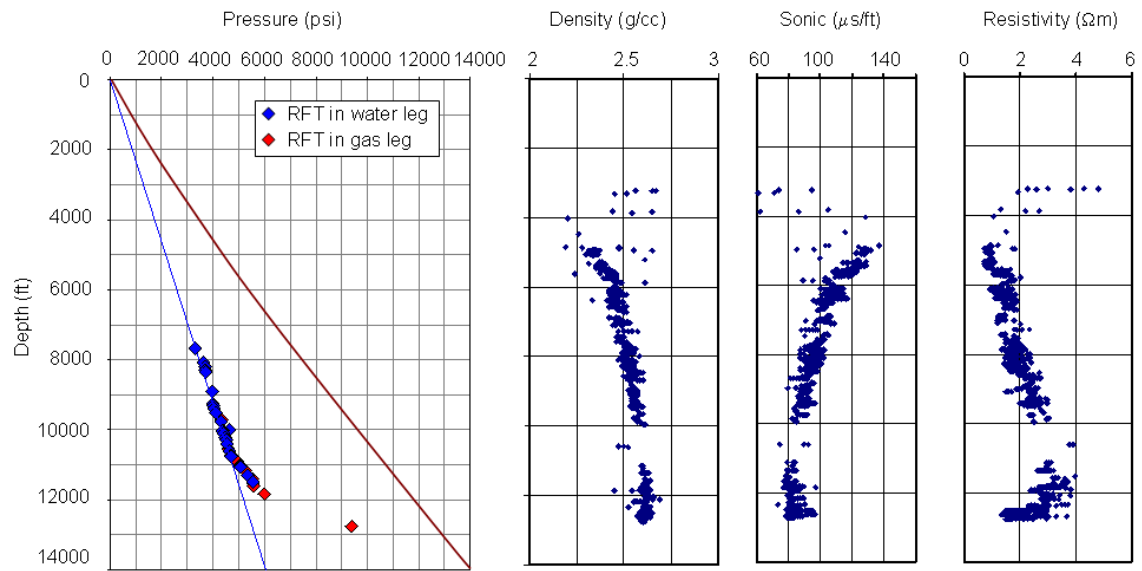
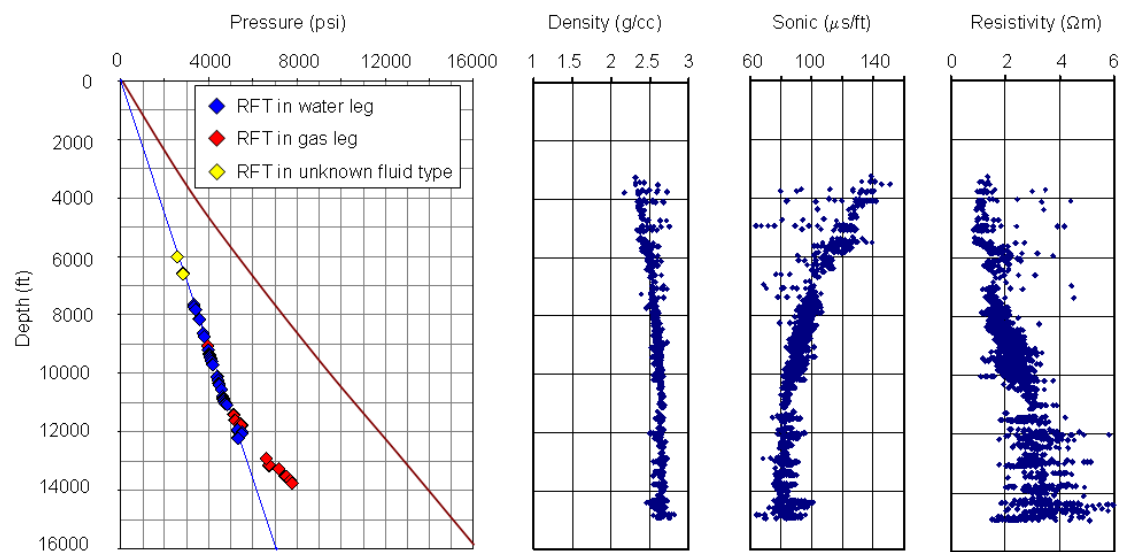Figure 9. Pressure-depth plot for well NWP-9 with density, sonic, and resistivity log data for the mudrocks.

Figure 10. Pressure-depth plot for well NWP-16 with density, sonic, and resistivity log data for the mudrocks.
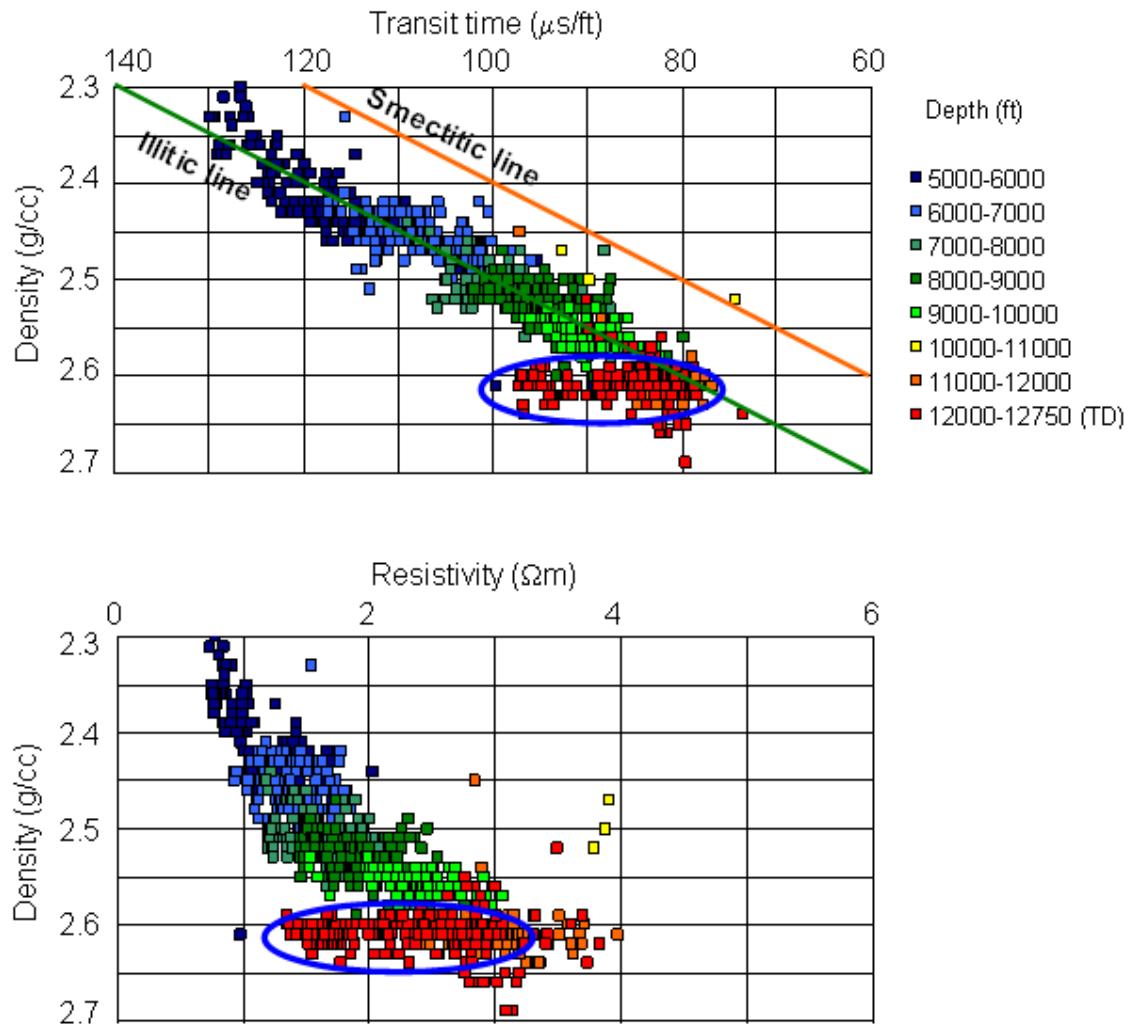
Figure 11. Crossplots of density against sonic transit time and resistivity for well NWP-9.

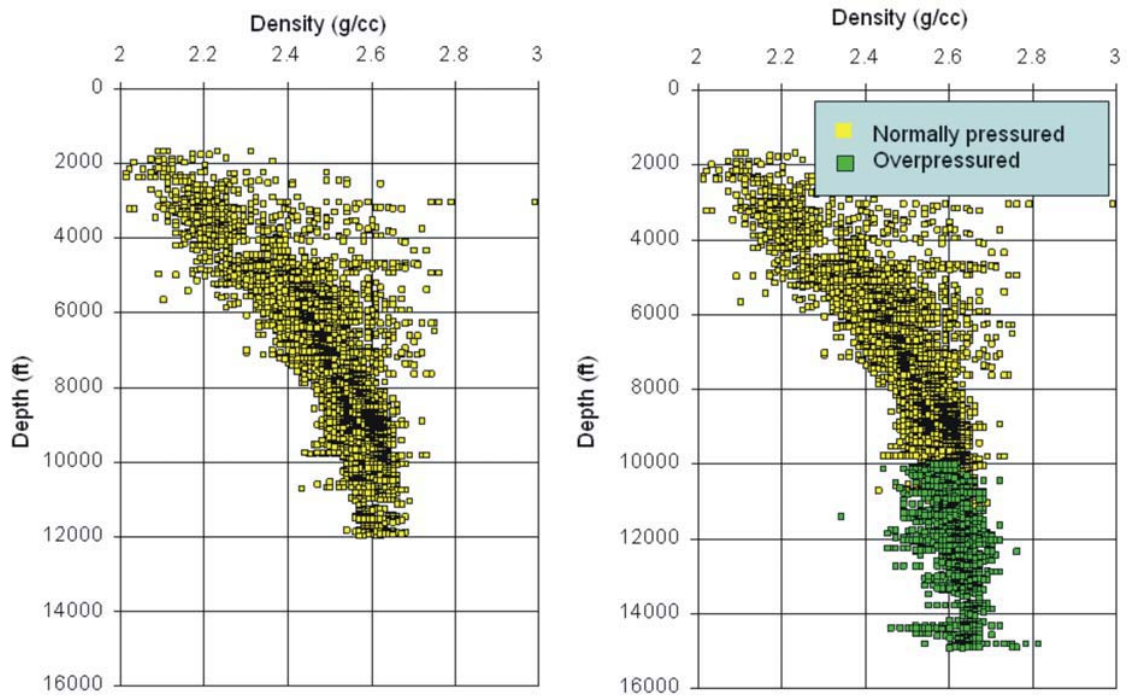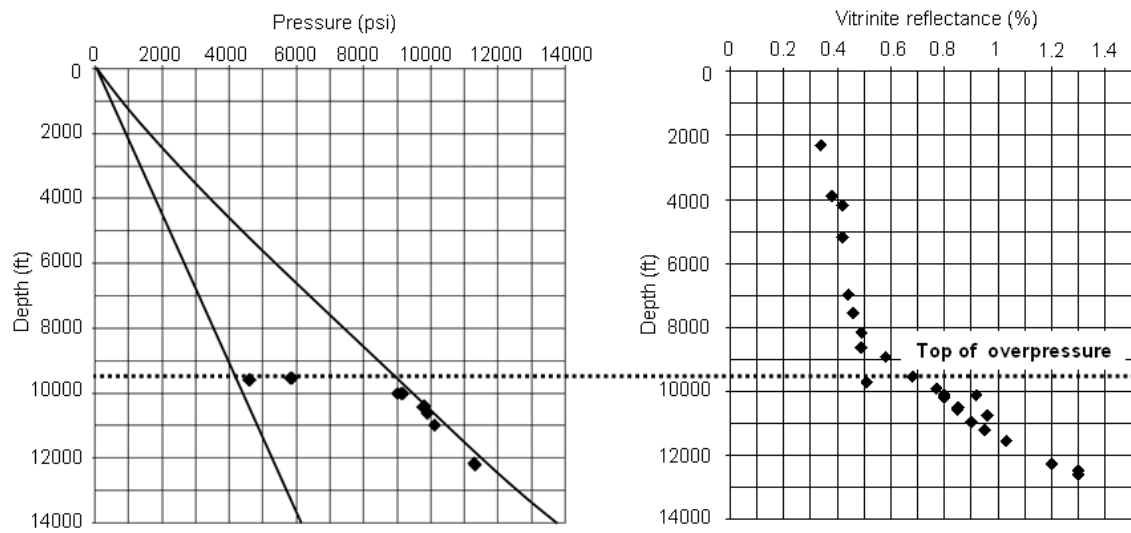Data points on unloading trends are encircled in blue.

Figure 12. Composite density plot for mudrocks, defined by NPHI – DPHI > 0.18, in all the NWP wells, Peciko Field: (a) for the hydrostatically pressured intervals only; and (b) for all the density log data.
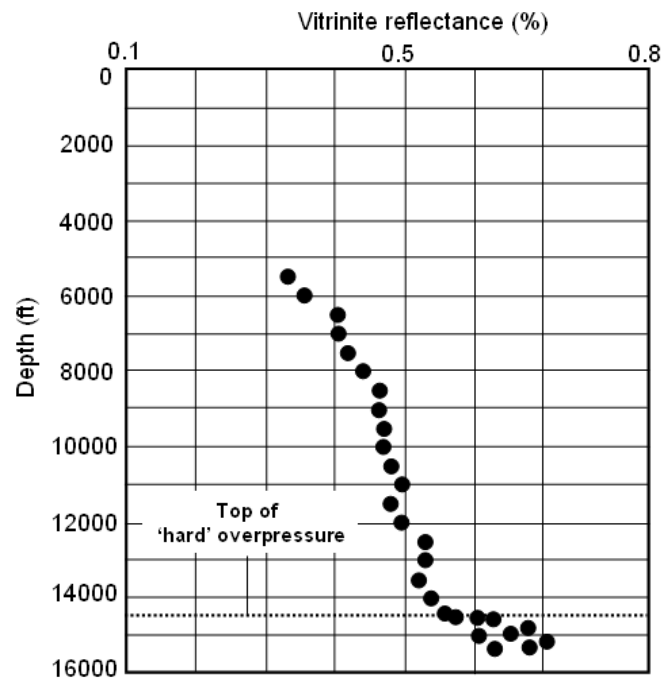
Figure 13. Vitrinite reflectance data and the pressure-depth plot from well H-9-B1 in the

Handil Field (location in Fig. 1). After Oudin & Picard (1982).

Figure 14. Vitrinite reflectance data from well N-109X in the Nilam Field (location in Fig. 1)

After Bates (1996).